crystals

MDPI

Article

Taking Advantage of the Coordinative Behavior of a Tridentate Schiff Base Ligand towards Pd^{2+} and Cu^{2+}

Jesús Sanmartín-Matalobos [1,*], Matilde Fondo [1], Morteza Zarepour-Jevinani [1,2] and Ana M. García-Deibe [1]

[1] Departamento de Química Inorgánica, Facultad de Química, Universidad de Santiago de Compostela, Avda. de las ciencias s/n, 15782 Santiago de Compostela, Spain
[2] Department of Chemistry, Sharif University of Technology, Tehran P.O. Box 11155-3516, Iran
* Correspondence: jesus.sanmartin@usc.es

Received: 23 July 2019; Accepted: 3 August 2019; Published: 5 August 2019

Abstract: We have explored the suitability of an *O,N,N*–donor Schiff base (H_2SB) for obtaining dinuclear complexes with heavy metal ions such as Cu^{2+}, Zn^{2+}, Ni^{2+}, and Co^{2+} (borderline acids) as well as Pd^{2+} and Cd^{2+} (soft acids). Spectroscopic studies demonstrated that the complexation of H_2SB and Cu^{2+}, Zn^{2+}, Ni^{2+}, Co^{2+}, Pd^{2+}, and Cd^{2+} occurred at a 1:1 stoichiometry. We have found two square planar centers with Pd-N-Pd angles of 93.08(11)° and a Pd–Pd distance of 3.0102(4) Å in $Pd_2(SB)_2{\cdot}Me_2CO$. This Pd–Pd distance is 30% shorter than the sum of the van der Waals radii, which is in accordance with a strong palladophilic interaction. Fluorescence studies on H_2SB-M^{2+} interaction showed that H_2SB can detect Cu^{2+} ions in a sample matrix containing various metal ions (hard, soft, or borderline acids) without interference. Determination of binding constants showed that H_2SB has a greater affinity for borderline acids than for soft acids.

Keywords: X-ray; fluorescence; metallophilic interaction; palladium; copper; Schiff base

1. Introduction

Metallophilic interactions have attracted the interest of many researchers because they can lead to the formation of supramolecular assemblies of metal complexes, as dimers, oligomers, chains, or sheets, showing useful properties [1–10]. These M···M interactions, which can be as strong as hydrogen bonds, can lead to M–M distances shorter than the sum of the van der Waals radii, facilitating the electronic communication between heavy metal atoms. Among these short contacts, d^{10}-d^{10} and d^8-d^8 interactions have aroused considerable interest, especially when the metal ions involved belong to the second and third transition series. This is because some of them exhibit unique optical, magnetic, chemical, photochemical, or catalytic properties. In particular, dinuclear complexes with palladophilic interactions have demonstrated versatile uses both in catalysis and in synthetic organic chemistry [11–14]. Despite this potential interest, very little research has been devoted to the synthesis of dinuclear palladium(II) complexes through μ_2–*N* bridges with short contacts. Thus, a search in Cambridge Structural Database data [15] indicates that, among more than a million of crystal structures already deposited, only eleven dinuclear palladium complexes connected through μ_2–*N* bridges display Pd–Pd distances shorter than 3.02 Å [16–25]. Figure 1 shows the four types of μ_2–*N* bridges so far reported in literature.

Recently, we have reported the crystal structures of two dinuclear palladium(II) complexes, with Pd–Pd distances in the range 3.00–3.02 Å [24,25]. These short interatomic distances were achieved by using tridentate Schiff bases that simultaneously bind two Pd^{2+} ions through μ_2–$N_{sulphonamido}$ bridges. As a continuation of our investigation, we report herein the synthesis and characterization of a new Schiff base (H_2SB, Figure 1) incorporating a suitable *O,N,N*-binding domain with the aim of

obtaining dinuclear complexes with heavy metal ions such as Cu^{2+}, Zn^{2+}, Ni^{2+}, and Co^{2+} (borderline acids) as well as Pd^{2+} and Cd^{2+} (soft acids) through a double μ_2–$N_{sulphonamido}$ bridge (Figure 1, right). Spectroscopic studies demonstrated that the complexation of H_2SB and Cu^{2+}, Zn^{2+}, Ni^{2+}, Co^{2+}, Pd^{2+}, and Cd^{2+} occurred at a 1:1 stoichiometry. The crystal structure of $Pd_2(SB)_2{\cdot}Me_2CO$, which has been elucidated by using single crystal X-ray diffraction techniques, has shown a Pd–Pd distance of 3.0102(4) Å, which is sensibly shorter than the sum of the van der Waals radii (4.30 Å). This latter value corresponds to that deduced from recent statistical analyses of intermolecular contacts in deposited X-ray crystal structures, paying also special attention to homoatomic contacts involving Pd, Pt, Cu, Ag, and Au [26]. Fluorescence studies on the interaction of H_2SB towards heavy metal ions such as Cu^{2+}, Zn^{2+}, Ni^{2+}, Co^{2+}, Cd^{2+}, and Pd^{2+} revealed the ability of H_2SB to detect Cu^{2+} in aqueous solutions containing various metal ions (hard, soft, or borderline acids) without interference. Determination of binding constants showed that H_2SB has a greater affinity for borderline acids than for soft acids.

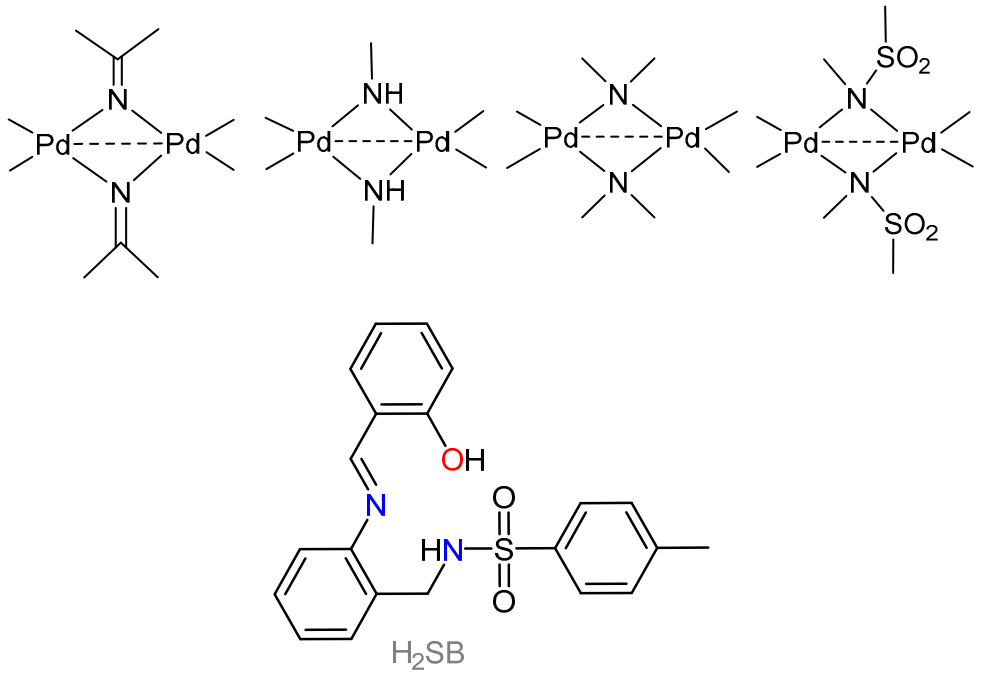

Figure 1. Schematic representation of the μ_2–*N* bridges reported for dinuclear palladium complexes crystallographically characterized (top), and the tridentate Schiff base H_2SB used in this work (bottom).

2. Experiment

2.1. Materials and Methods

The starting materials and reagents were commercially available and were used without further purification. The synthesis of the starting sulphonamide 2–tosylaminomethylaniline, which derives from the reaction of 2–aminobenzylamine with tosyl chloride has been previously reported [27]. Elemental analyses were performed on a Thermo Finnigan analyzer (Flash 1112). Mass spectra were recorded using FAB or MALDI-TOF techniques. Partial views of the mass spectra of the compounds are shown in SM (Supplementary Materials Figures S1–S5). Infrared spectra were recorded as KBr pellets on a Jasco FT/IR-410 spectrophotometer (JASCO Inc, Easton, MD USA) in the range 4000–600 cm^{-1} (Figures S6–S11). ^1H NMR spectra (400 MHz, Varian Inova 400, Varian Medical Systems, Inc. Palo Alto, CA; USA) and ^{13}C NMR spectra (100 MHz, Varian Inova 400, Varian Medical Systems, Inc. Palo Alto, CA; USA) were measured in deuterated solvents. *J* values are given in Hertz. NMR assignments were carried out by a combination of COSY, NOESY, HSQC and HMBC experiments. The NMR numbering scheme is the same that we have used in the molecular structure of H_2SB. Partial views

of the NMR spectra of the diamagnetic compounds are shown in SM (Figures S12–S14). UV-Vis spectra were recorded using an Uvikon 810 spectrophotometer (Kontron Instruments, Ismaning Germany) (Figure S15). Fluorescence spectra were recorded on a Fluoromax-2 spectrofluorometer (Jobin Yvon-Spex, Edison, NJ, USA).

2.2. Crystal Structure Analysis Data

Diffraction data for H_2SB and $Pd_2(SB)_2{\cdot}Me_2CO$ were collected at 100(2) K, using graphite-monochromatized Mo-Kα radiation (λ = 0.71073 Å) from a fine focus sealed tube. Main crystal parameters and refinement data are listed in Table S1. Data were processed and corrected both for Lorentz and polarization effects. Multi-scan absorption corrections [28] were performed using the SADABS routine [29]. The structures were solved by standard direct methods [30] and then refined by full matrix least squares on F^2 [30]. All non-hydrogen atoms were anisotropically refined, while most of the H atoms were included in the structure factor calculation in geometrically idealized positions, by using a riding model with thermal parameters depending of the parent atom. Those H atoms that could be involved in a classic H bonding scheme for H_2SB were located on Fourier maps, and isotropically treated. Figure S16 shows mutual intermolecular interactions between neighboring molecules of H_2SB.

2.3. Synthesis of H_2SB

2–hydroxybenzaldehyde (0.16 mL, 1.45 mmol) was added to 2–tosylaminomethylaniline solved in absolute ethanol solution (40 mL) of [27] (0.40 g, 1.45 mmol) and the resulting solution was refluxed for 4 h. After cooling, the resulting solution was concentrated to obtain a yellowish oily product. A hexane solution of the oily product (20 mL) was stirred overnight, and the resulting yellow solid was filtrated and dried under vacuum. Yellow prismatic crystals of H_2SB suitable for single-crystal X-ray studies were obtained by recrystallization of a chloroform solution of the reaction crude. Yield = 0.50 g (90%). MS (FAB^+, MNBA) m/z (%) [adduct]: 381.2 (100) $[H_2SB+H]^+$. ^{1}H NMR (500 MHz, dmso-d_6, δ in ppm): 12.48 (s, 1H, HO20), 8.74 (s, 1H, H14), 8.03 (t, *J* = 5.9 Hz, 1H, HN), 7.65 (d, *J* = 8.2 Hz, 1H, H16), 7.64 (d, *J* = 8.2 Hz, 1H, H2 + H6), 7.44 (t, *J* = 8.2 and 1.0 Hz, 2H, H18), 7.38 (d, *J* = 8.0 Hz, 1H, H9), 7.36 (t, *J* = 8.0 Hz, 1H, H11), 7.31 (d, *J* = 8.2 Hz, 2H, H3 + H5), 7.25 (t, *J* = 7.4 Hz, 1H, H10), 7.22 (d, *J* = 7.4 Hz, 2H, H12), 7.00 (t, *J* = 7.6 Hz, 1H, H17), 6.97 (d, *J* = 7.8 Hz, 1H, H19), 4.08 (d, *J* = 6.0 Hz, 2H, H7), 2.35 (s, 3H, H40). ^{13}C NMR (125 MHz, dmso-d_6, δ in ppm): 164.4 (C14), 160.5 (C20), 147.6 (C13), 142.9 (C4), 138.1 (C1), 133.9 (C18), 132.9 (C16), 131.2 (C8), 130.0 (C3 + C5), 129.3 (C9), 129.0 (C11), 126.8 (C10), 126.8 (C2 + C6), 120.0 (C15), 119.5 (C17), 119.0 (C12), 117.1 (C19), 42.4 (C7), 21.4 (C40). IR (KBr, ν/cm^{-1}): ν(OH) 3296, ν(NH) 3268, ν(C=N_{imi}) 1616, $\nu_{as}(SO_2)$ 1328, $\nu_s(SO_2)$ 1163. Elemental analysis (found): C 66.0; H 5.5; N 7.5; S 8.4%; calc. for $C_{21}H_{20}N_2O_3S$: C 66.3; H 5.3; N 7.4; S 8.4%.

2.4. Synthesis of $Pd_2(SB)_2$

A methanol solution (40 mL) of $Pd(OAc)_2{\cdot}4H_2O$ (0.10 g, 0.39 mmol) and H_2SB (0.15 g, 0.39 mmol) was stirred overnight at room temperature. An orange precipitate was filtered off, washed with methanol and then dried under vacuum. Orange rhombic crystals of $Pd_2(SB)_2{\cdot}Me_2CO$ suitable for single-crystal X-ray studies were obtained by recrystallization in acetone. Yield = 0.14 g (73%). MS (FAB+, MNBA) m/z (%) [adduct]: 970.7 (26) $[Pd_2(SB)_2+H]^+$. ^{1}H NMR (500 MHz, dmso-d_6, δ in ppm): 8.10 (s, 2H, H14), 7.57 (d, 2H, H16), 7.52 (d, 4H, H2+H6), 7.39 (t, 2H, H18), 7.15 (t, 2H, H10), 7.14 (t, 2H, H11), 7.12 (d, 2H, H9), 6.95 (d, 2H, H19), 6.88 (d, 4H, H3 + H5), 6.71 (d, 2H, H12), 6.68(t, 2H, H17), 4.12 (s, 4H, H7), 2.20 (s, 6H, H40). IR (KBr, ν in cm^{-1}): ν(C=N_{imine}) 1585, $\nu_{as}(SO_2)$ 1327, $\nu_s(SO_2)$ 1156. Elemental analysis (found): C 52.2; H 4.0; N 5,7; S 6.5%; calc. for $C_{42}H_{36}N_4O_6Pd_2S_2$: C 52.0; H 3.7; N 5.8; S 6.6%.

2.5. Synthesis of $Cd_2(SB)_2$

A methanol solution (40 mL) of H_2SB (0.10 g, 0.26 mmol) and $Cd(OAc)_2{\cdot}2H_2O$ (0.07 g, 0.26 mmol) was stirred overnight at room temperature. The resulting solution was concentrated to obtain an oily product. This latter product was stirring with 10 mL of diethyl ether during 4 hours to yield a precipitate. Then it was filtrated obtaining a yellow precipitate that was air-dried. Yield: 0.08 g (67%). ^{1}H NMR (500 MHz, dmso-d_6, δ in ppm): 8.23 (s, 1H, H14), 7.68 (d, *J* = 8.1 Hz, 2H, H2 + H6), 7.25 (t, *J* = 5.6 Hz, 1H, H11), 7.16 (d, *J* = 8.1 Hz, 2H, H3 + H5), 7.12 (t, 1H, H10), 7.01 (d, *J* = 6.3 Hz, 1H, H16), 6.91 (d, *J* = 7.4 Hz, 1H, H9), 6.86 (d, *J* = 6.7 Hz, 1H, H19), 6.59 (d, *J* = 7.0 Hz, 1H, H12), 6.39 (t, *J* = 7.2 Hz, 1H, H17), 4.22 (s, 2H, H7), 2.29 (s, 3H, H40). IR (KBr, ν in cm^{-1}): ν(C=N) 1612, $\nu_{as}(SO_2)$ 1343, $\nu_s(SO_2)$ 1156. Elemental analysis (found): C 51.0; H 3.5; N 5.6; S 6.2%; calc. for $C_{21}H_{18}CdN_2O_3S$: C 51.4; H 3.7; N 5.7; S 6.5%.

2.6. Synthesis of $Zn_2(SB)_2{\cdot}4H_2O$

A methanol solution (40 mL) containing H_2SB (0.10 g, 0.26 mmol) and $Zn(OAc)_2{\cdot}2H_2O$ (0.06 g, 0.26 mmol) was stirred overnight at room temperature. The resulting solution was concentrated to obtain an oily product. This dense oil was stirred with 20 mL of diethyl ether during 30 minutes. The resulting suspension was filtrated and washed with acetonitrile obtaining a yellow precipitate that was air-dried. Yield: 0.05 g (86%). ^{1}H NMR (250 MHz, dmso-d_6, δ in ppm): 8.50 (s, 1H, H14), 7.66 (d, *J* = 7.6 Hz, 2H, H2 + H6), 7.40 (d, *J* = 7.6 Hz, 1H, H19), 7.34 (d, *J* = 8.2 Hz, 1H, H16), 7.30 (t, 1H, H11), 7.22 (d, *J* = 7.6 Hz, 2H, H3 + H5), 7.16 (t, 1H, H18), 7.12 (t, *J* = 5.3 Hz, 1H, H10), 7.09 (d, 1H, H9), 6.77 (d, *J* = 8.8 Hz, 1H, H12), 6.59 (t, *J* = 7.6 Hz, 1H, H17), 3.90 (s, 2H, H7), 2.30 (s, 3H, H40). IR (KBr, ν in cm^{-1}): ν(C=N) 1616, $\nu_{as}(SO_2)$ 1395, $\nu_s(SO_2)$ 1150. Elemental analysis (found): C 52.3; H 4.3; N 5.7; S 6.4%; calc. for $C_{21}H_{22}N_2O_5SZn$: C 52.6; H 4.6; N 5.8; S 6.7%.

2.7. Synthesis of $Ni_2(SB)_2{\cdot}4H_2O$

A methanol solution (40 mL) of $Ni(OAc)_2{\cdot}4H_2O$ (0.07 g, 0.26 mmol) and H_2SB (0.10 g, 0.26 mmol) was stirred overnight at room temperature. The resulting solution was concentrated to obtain an oily product. This latter one was stirried with 20 mL of diethyl ether during 30 minutes. The resulting precipitate was filtered off and then air-dried. Yield = 0.09 g (73%). MS (MALDI-TOF$^+$, DCTB) *m/z* (%) [adduct]: 875.0 (80) $[Ni_2(SB)_2+H]^+$. IR (KBr, ν in cm^{-1}): ν(OH) 3436, ν(C=N) 1608, $\nu_{as}(SO_2)$ 1315, $\nu_s(SO_2)$ 1160. Elemental analysis (found): C 53.3; H 4.6; N 5.6; S 7.1 %; calc. for $C_{42}H_{44}Ni_2N_4O_{10}S_2$: C 53.3; H 4.7; N 5.9; S 6.8%.

2.8. Synthesis of $Cu_2(SB)_2{\cdot}2MeOH$

A methanol solution (40 mL) of H_2SB (0.10 g, 0.26 mmol) and $Cu(OAc)_2{\cdot}H_2O$ (0.06 g, 0.26 mmol) was stirred overnight at room temperature. The resulting suspension was filtered off and then air-dried. Yield: 0.04 g (73%). MS (MALDI-TOF, DCTB) *m/z*: 947.0 (27) $[Cu_2(SB)_2(MeOH)_2+H]^+$. IR (KBr, ν in cm^{-1}): ν(OH) 3435, ν(C=N) 1585, $\nu_{as}(SO_2)$ 1327, $\nu_s(SO_2)$ 1156. Elemental analysis (found): C 55.2; H 4.5; N 5.6; S 7.0%; calc. for $C_{44}H_{44}Cu_2N_4O_8S_2$: C 55.7; H 4.7; N 5.9; S, 6.8%.

2.9. Synthesis of $Co_2(SB)_2{\cdot}4H_2O$

A methanol solution (40 mL) of H_2SB (0.10 g, 0.26 mmol) and $Co(OAc)_2{\cdot}4H_2O$ (0.07 g, 0.26 mmol) was stirred overnight at room temperature. The resulting solution was concentrated to obtain an oily product. This product was stirred with 20 mL of diethyl ether during 30 minutes. The resulting precipitate was filtered off and then dried under vacuum. Yield = 0.05 g (41%). MS (MALDI-TOF, DCTB) *m/z* (%) [adduct]: 875.0 (100) $[Co_2(SB)_2+H]^+$. IR (KBr, ν in cm^{-1}): ν(OH) 3438, ν(C=N) 1611, $\nu_{as}(SO_2)$ 1335, $\nu_s(SO_2)$ 1157. Elemental analysis (found): C 53.0; H 4.5; N 5.8; S 6.4%; calc. for $C_{42}H_{44}Co_2N_4O_{10}S_2$: C 53.3; H 4.7; N 5.9; S 6.8%.

3. Results and Discussion

With the aim of understanding the potential bonding behavior of H_2SB upon binding different metal ions, we need to know the corresponding binding stoichiometry, degree of deprotonation, and coordination environment. Therefore, we synthesized some representative dinuclear complexes with soft and borderline acids, and then, we studied their behavior in solution by a combination of NMR, UV-Vis, and mass spectrometries. The bonding situation was also investigated in the solid state, by elemental analysis, FT-IR spectroscopy, and X-ray diffraction. The crystal structures of H_2SB and $Pd_2(SB)_2 \cdot Me_2CO$ were determined by using single crystal X-ray diffraction techniques.

3.1. Crystal Structure of H_2SB

Single crystal X-ray diffraction techniques have demonstrated that the imine group of H_2SB displays a typical *E* configuration for a Schiff base with a hydroxyl group *ortho* positioned (Figure 2). This configuration is favored by an intramolecular O3–H3···N2 interaction, with a length of only 2.607(3) Å. This short distance evidences its intensity, and it could be qualified as strong intramolecular resonance-assisted H-bond [31]. The torsion of 165.00(16)° found for the C8–C7–N1–S1 bonds indicates a typical *anti* conformation of the sulphonamide group in this free ligand, with an angle higher than some others found for several conformers of a related ligand also derived from 2-tosylaminomethylaniline [27]. The torsion of C6–C1–S1–N1 (−90.6(2)°) illustrates the almost perpendicular disposition of the tolyl ring with respect to the N1–S1 bond, and which is typical of this group in this kind of compound [27]. Meaningful bond distances and angles (Table S2) also fall within the usual ranges found for other 2-tosylaminomethylaniline derivatives [32,33].

With regard to the packing scheme of this free ligand, some intermolecular interactions occur between the sulphonamide groups of neighboring molecules to associate them in pairs (Figure S16), through two mutual N1–H1A···O1 interactions (Table S3). Association in pairs so related is relatively common for free sulphonamide ligands [27]. Furthermore, these couples of molecules are forming 1D chains, as they are consecutively connected by means of π-π stacking, with neighboring pairs related by an inversion center. Thus, each flat conjugated fragment formed by the imine group connecting the C8–C13 and the C15–C20 phenyl rings, are stacked with another inverted fragment), being the distance between their respective centroids of 3.77(2) Å.

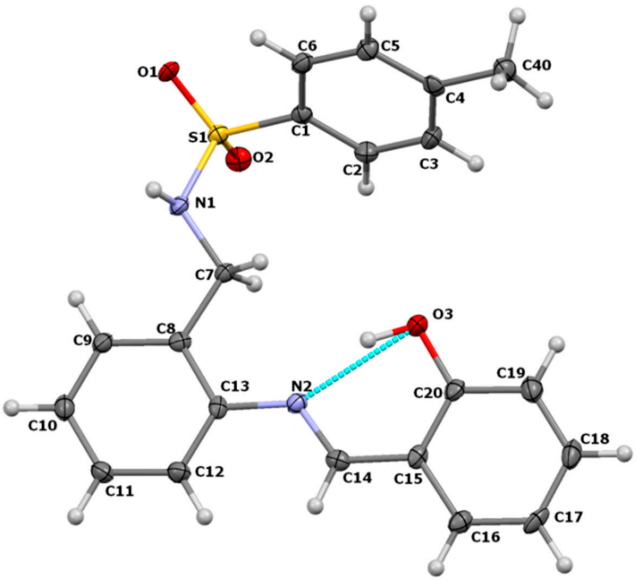

Figure 2. Ellipsoid view (50% probability) of the molecular structure of H_2SB with the numbering scheme. The interaction between donor and acceptor atoms in the intramolecular H bond is represented as a dotted light blue line.

3.2. Crystal Structure of $Pd_2(SB)_2 \cdot Me_2CO$

The molecular structure of the neutral dimeric palladium(II) complex present in the crystal structure of $Pd_2(SB)_2 \cdot Me_2CO$ is shown in Figure 3 as an ellipsoid diagram, which includes its labelling scheme, but excludes its H atoms for clarity. The main geometric parameters of this compound are listed in Table S4. Coordination distances Pd–O and Pd–N are ranging 1.971(2)–1.972(2) Å and 2.022(3)–2.103(3) Å, respectively, so they can be considered within the usual ranges found for other related compounds [24,25,34]. By contrast, Pd–O_{tosyl} distances are longer (3.035(2) and 3.129(2) Å), what reflects very weak metal–ligand interactions, so that they cannot be qualified as true coordination bonds. Hence, $Pd_2(SB)_2$ shows two pseudo-square planar centers with Pd-N-Pd angles of 92.68(10) and 93.08(11), while the Pd–Pd distance is 3.0102(4) Å (Figure 4). This Pd–Pd distance is 30% shorter than the sum of the van der Waals radius (4.30 Å) [26], and it is in accordance with a rather intense palladophilic interaction [26], and illustrated in Figure S16 of the supplementary information. Figure S16 also reflects the angle formed by both almost planar N_2O_2 donor sets around the palladium ions, which is of 32.9(2)°, considering the calculated planes formed by these atoms. The marked planarity is demonstrated by the low deviations of these atoms from these planes, as the maximum distance 0.122(2) Å, which corresponds to that between Pd1 and the plane calculated for its chromophore.

In spite of the considerable steric hindrance that both bulky tosyl groups can exert, they are oriented towards the same side of the mentioned Pd_2N_2 metallacycle, what could be considered as a *syn* disposition, involving a C_{2v} molecular symmetry (Figure 3). By contrast with the free ligand, after coordination, these tosyl groups are folded in such way that the p-tolyl rings are practically π–π stacked under those of their respective salicylaldehyde residues, with a distance between their centroids of 3.62(2) and 3.77(2) Å. With this disposition, the palladium ions can be accessible for potential substrates in its hypothetical use as a catalyst. The Pd–$N_{sulphonamide}$ distances (in the range 2.057(3)–2.103(3) Å are longer than the Pd–N_{imine} ones. This fact evidences some lability for μ_2–N bridges is evidenced [24,25]. This is a highly valued structural feature in catalysis because the break of the Pd–$N_{sulphonamide}$ bound could allow the access of a substrate to the reaction site.

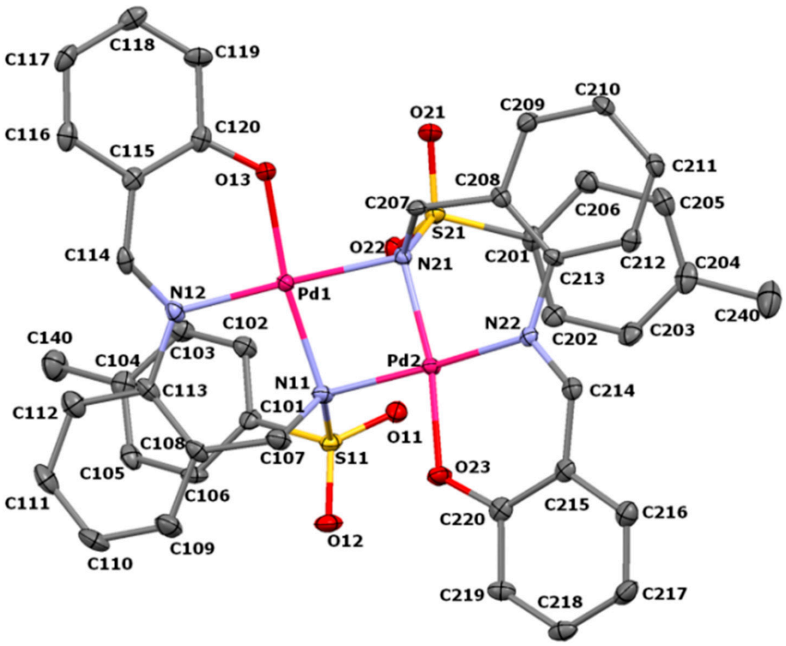

Figure 3. Ellipsoid view (50% of probability) of the molecular structure of $Pd_2(SB)_2 \cdot Me_2CO$. H atoms and the solvated acetone molecule have been omitted for clarity.

3.3. Spectroscopic Characterization of the Non-Crystalline Complexes

The dinuclear nature of the non-crystalline complexes $Cu_2(SB)_2{\cdot}2MeOH$, $Ni_2(SB)_2{\cdot}4H_2O$, and $Co_2(SB)_2{\cdot}4H_2O$ was deduced on the basis of mass spectrometry data. Figures S2 and S3 show the peaks attributed to the molecular ion $[M_2(SB)_2+H]^+$, which were observed in the mass spectra of $Co_2(SB)_2{\cdot}4H_2O$ and $Ni_2(SB)_2{\cdot}4H_2O$, respectively. Since we have detected the adduct $[Cu_2(SB)_2(MeOH)_2+H]^+$ in the mass spectrum of $Cu_2(SB)_2{\cdot}2MeOH$, a methanol molecule seems to be present in the coordination sphere of each Cu^{2+} ion. The electronic absorption spectrum of $Cu_2(SB)_2{\cdot}2MeOH$ (in methanol) showed a broad, but low intensity d-d band, centered near 670 nm (Figure S15), which is coherent with a square-pyramidal CuN_3O_2 coordination geometry [35].

Bideprotonation of the ligand in dinuclear complexes is easy to deduce because ν(NH) and ν(OH) bands at about 3268 and 3296 cm^{-1}, respectively, are absent in their infrared spectra (Figures S6–S11). Regarding to the ^1H NMR spectra of $Zn_2(SB)_2{\cdot}4H_2O$, $Cd_2(SB)_2$, and $Pd_2(SB)_2$, these show the absence of OH and NH signals, what supports that the ligand is coordinated as a dianionic species. This can be clearly observed in Figure 4. The signal corresponding to the –CH=N group can be also observed at about 8.7 ppm in the free ligand, while for the coordinated SB^{2-} undergoes a shift to the high field (about 0.2–0.5 ppm), indicating the coordination of the ligand through the imine nitrogen atom.

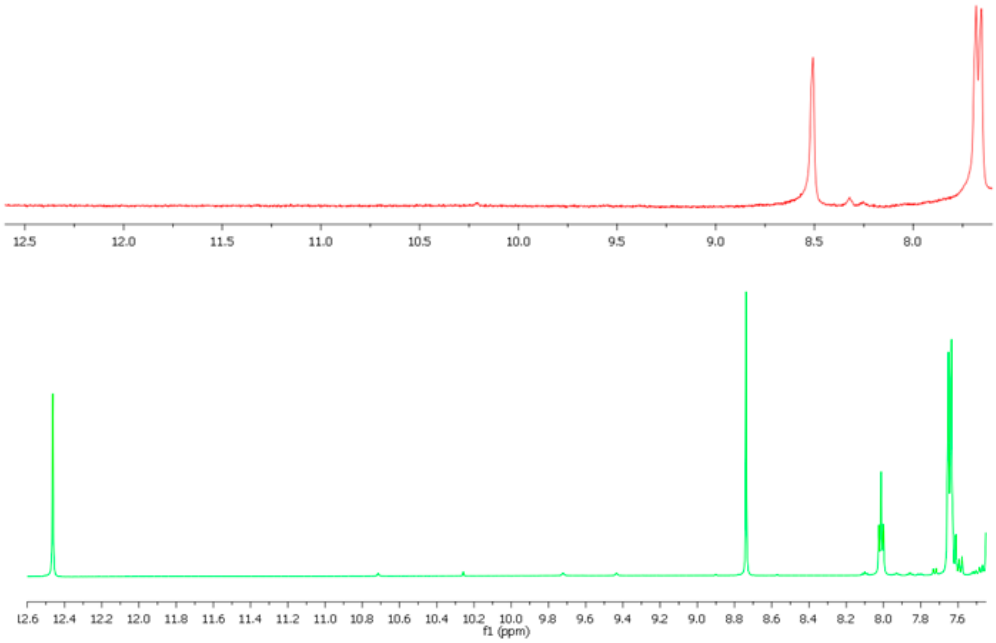

Figure 4. Partial view of the ^1H NMR spectra of H_2SB (bottom) and $Zn_2(SB)_2{\cdot}4H_2O$ (top).

3.4. UV-Vis Studies on the H_2SB-M^{2+} Interaction

We have studied the changes in the UV-Vis spectrum of H_2SB upon titration with heavy metal ions such as Cu^{2+}, Zn^{2+}, Ni^{2+}, and Co^{2+} (borderline acids) as well as Pd^{2+} and Cd^{2+} (soft acids). In the absence of metal ions, H_2SB displayed four intense intraligand absorption bands with centers at about 204, 228, 270, and 340 nm. These bands result from π→π* and n→π* transitions of the conjugated system (Figure 5).

The most remarkable spectral change observed as a result of the complexation of H_2SB with Cu^{2+}, Co^{2+}, Ni^{2+}, Zn^{2+}, and Cd^{2+} (Figures S18–S21) was the appearance of an additional absorption band at about 390 nm (MLTC), which was not observed after Pd^{2+} complexation (Figure S22). Besides, the n →π* transition related to the azomethine group underwent a red (bathochromic) shift from 270 to 285 nm, as a consequence of Cu^{2+} complexation (Figure 7), which was attributed to an increase in the electron density at the imine nitrogen atom. This is also observed, although with a lesser extent,

after Zn^{2+} complexation (10 nm red shift), being the shift even lesser with the remaining metal ions. In contrast, after addition of Pd^{2+} ions there are very little changes related to the intraligand absorption bands of H_2SB, which is probably due to not significant changes in the electron density at donor atoms as a consequence of palladium complexation. Based on that, we speculated that perhaps H_2SB-Cu^{2+} could be the strongest interaction and H_2SB-Pd^{2+} the weakest one.

In order to find out the binding stoichiometry of the complexes obtained by interaction of H_2SB with M^{2+} ions, Job's plot method was used. Analysis of the UV-Vis data for complexation of H_2SB with M^{2+} (Cu^{2+}, Zn^{2+}, Ni^{2+}, Co^{2+} Pd^{2+}, and Cd^{2+}) supports the 1:1 stoichiometry that was found in the characterized complexes (Figure S23).

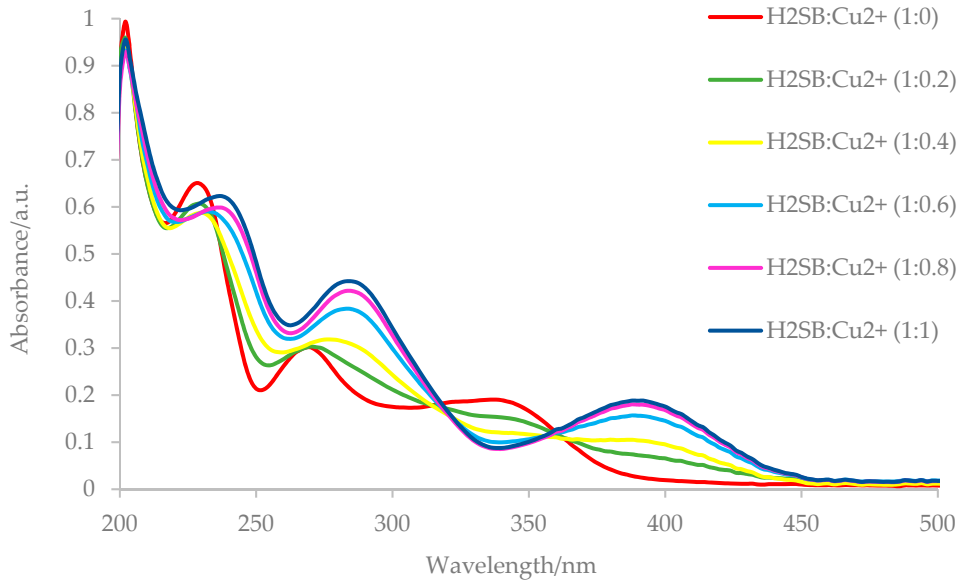

Figure 5. Partial view of the absorption spectra of H_2SB (100 μM,) before (red line) and after addition of Cu^{2+} (100 μM), measured in methanol-water in 80:20 v/v (pH 7.0–7.5). Spectral data were recorded immediately after the addition of Cu^{2+} (0.0, 0.2, 0.4, 0.6, 0.8, and 1.0 mL) to H_2SB (1.0 mL) at room temperature.

3.5. Fluorescence Studies on the H_2SB-M^{n+} Interaction

Exposition to UV light with a wavelength of 390 nm of an aqueous solution of H_2SB emitted a maximal fluorescence at about 500 nm (Figure 6). The fluorescence intensity of H_2SB depends on the pH, as it experiments a drastic increase at pH values higher than 11, whereas pH values in the range 4.0 to 9.5 exert scarce influence on the fluorescence intensity. Since pK_a of -OH and $–SO_2$-NH- groups have values near to 10, we have attributed this enhancement of the intensity to deprotonation of both acidic groups in H_2SB.

We speculated that a linear varying (enhancement or quenching) of the fluorescence intensity with increasing M^{n+} ion concentration, could allow the feasibility of H_2SB as a fluorescent probe for detection of any of the following heavy metal ions Cu^{2+}, Zn^{2+}, Ni^{2+}, Co^{2+}, Cd^{2+}, and Pd^{2+}. The subsequent studies showed that, in fact, enhancement of the fluorescence was observed upon titration with Zn^{2+} and Cd^{2+}, whereas titration with Co^{2+}, Ni^{2+}, Pd^{2+}, or Cu^{2+} led to partial quenching of the fluorescence (Figures S24–S28). Among these results, those observed in the presence of Cu^{2+} (declining intensity by over 90% after addition of 2.2 mg/L) have aroused our interest.

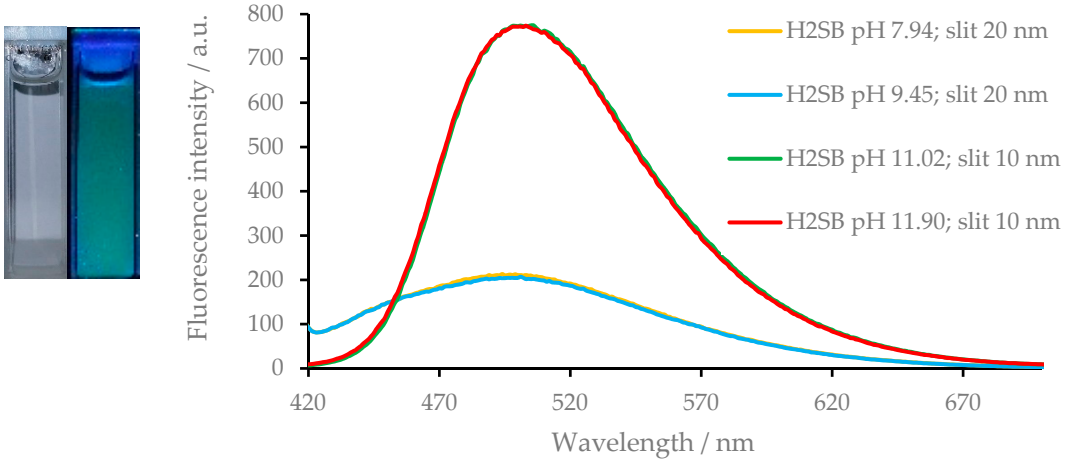

Figure 6. Left: Fluorescent photographic image under UV lamp (365 nm) obtained for the blue-emitting H_2SB (an image under daylight has been included to facilitate comparison). Right: Fluorescence spectrum of H_2SB (100 μM,) measured in methanol-water in 80:20 v/v at different pH values.

The variation in the fluorescence spectrum of H_2SB upon titration with Cu^{2+} ions are shown in Figure 7. The fluorescence intensity of H_2SB decreased with increasing Cu^{2+} ion concentration, in a methanol-water (in 80:20 v/v) solution. The fluorescence intensity varied linearly with the concentrations of Cu^{2+} ions in the range of 0 to 33 μM (0–2.1 mg/L), declining by over 90%. Since the detection limit for Cu^{2+} ions with H_2SB was 83 nM (5.3 μg L^{-1}), the working range was 0.276–33 μM (17.6–2.1 10^3 μg L^{-1}). Limits of detection and quantification were calculated according to the formula *LOD* = 3SD/b, LOQ = 10 SD/b, where SD is the standard deviation of the response, and b is the slope of the calibration curve. The quenching mechanism upon titration with Cu^{2+} ions was studied with Stern–Volmer plots ($I_0/I = 1 + K_{SV}$ $[M^{2+}]$) [36], and they are shown in Figure S29. From the slope, the values of the quenching constants (K_{SV}) for the H_2SB-Cu^{2+} interaction are found to be about 45.2 10^3 M^{-1} at 20°C, 39.4 10^3 M^{-1} at 30 °C, and 28.6 10^3 M^{-1} at 40°C. As increasing temperatures lead to a decrease of the quenching efficiency, quenching occurred as a result of a non-fluorescent ground-state complex formed between the fluorophore H_2SB and the quencher Cu^{2+} (static quenching). Hence, an increase in temperature appears to reduce the stability of the complex. It is noteworthy that, the binding constant for complex formation (K_b) is t he quenching constant K_{SV} for static quenching ($\tau_0/\tau = 1$).

The Benesi–Hildebrand equation [37] for 1:1 complexes has been used to determine the binding constant (K_b = intercept/slope) values of H_2SB with soft acids, such as Cd^{2+} and Pd^{2+} and borderline acids, such as Cu^{2+}, Zn^{2+}, Co^{2+}, and Ni^{2+}. The values of the binding constant at room temperature (K_b) of H_2SB with the Cu^{2+}, Zn^{2+}, Ni^{2+}, Co^{2+}, Cd^{2+}, and Pd^{2+} are found to be about 47.5 10^3, 38.5 10^3, 30.1 10^3, 26.7 10^3, 21.3 10^3, and 16.9 10^3 M^{-1}, respectively (Figure S30–S35). The good agreement between the value of the binding constant (at r.t.) calculated from Benesi–Hildebrand (47.5 10^3) and Stern–Volmer (45.1 10^3 M^{-1}) supports the accuracy of the calculations. Thus, we have found that the affinity of H_2SB for metal ions is according to the following series: Cu^{2+}>Zn^{2+}>Ni^{2+}>Co^{2+}>Cd^{2+}>Pd^{2+}. It must be noted that soft acids (Pd^{2+} and Cd^{2+}) are occupying the last positions, and borderline acids (Cu^{2+}, Zn^{2+}, Ni^{2+}, and Co^{2+}) occupy the first positions, with Cu^{2+} showing the highest affinity. Therefore, we will pay particular attention to the fluorescence study on the interaction between H_2SB and borderline acids, but especially on the H_2SB-Cu^{2+} interaction.

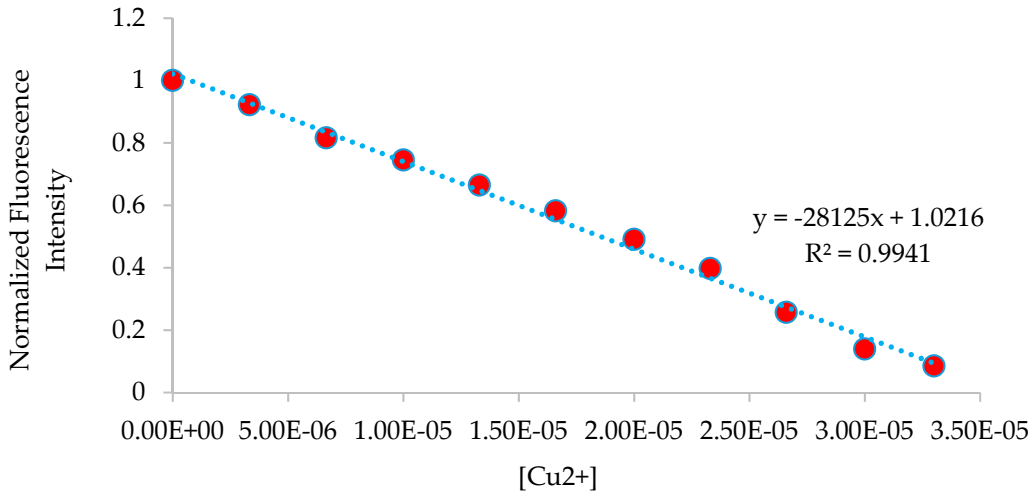

Figure 7. The linear relationship (trend line in blue) between fluorescence intensity and Cu^{2+} concentrations measured in methanol (pH 7.0–7.5) under λ_{exc} = 390 nm. Fluorescence intensity data have been rescaled to have values between 0 and 1. Spectral data were recorded at 5 minutes after the addition of Cu^{2+} (0.0, 0.1, 0.2, 0.3, 0.4, 0.5, 0.6, 0.7, 0.8, 0.9, and 1.0 mL) to H_2SB (1.0 mL) at r.t.

The selectivity of H_2SB as probe for the presence of Cu^{2+} ions was tested with several metal ions as interferents, including some other borderline acids, soft acids, and hard acids as well. A ±10% variation of the average luminescence intensity at the respective concentration of Cu^{2+} ions was used as a criterion for interference. These results showed that H_2SB is highly selective towards Cu^{2+}, even in the presence of metal ions as Na^+, K^+, Ag^+, Mg^{2+}, Ca^{2+}, Ba^{2+}, Mn^{2+}, Fe^{2+}, Co^{2+}, Ni^{2+}, Pd^{2+}, Zn^{2+}, Cd^{2+}, Mn^{3+}, Fe^{3+}, and Al^{3+}, which can be present with a 100 μmol L^{-1} concentration (Figure 8). To check the feasibility of H_2SB as probe for Cu^{2+} in real water samples, we also measured the fluorescence intensity of tap water. The results showed that the measured value 0.05 mg/L (0.72 μM) was far below the World Health Orgaization acceptable limit, which is 2.0 mg/L (31.5 μM) in drinking water.

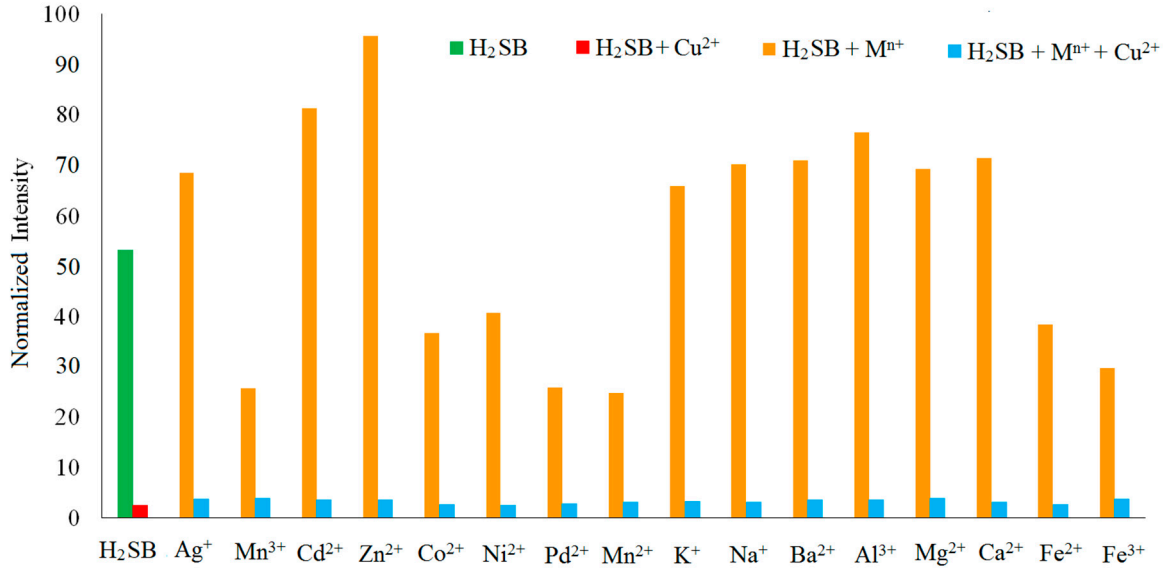

Figure 8. Fluorescence responses of H_2SB (1.0 mL, 100 μM) toward Cu^{2+} (1.0 mL, 100 μM) in the presence of various metal ions (1.0 mL, 100 μM). Fluorescence intensity data have been rescaled to have values between 0 and 100. All experiments were performed in methanol-water in 80:20 v/v (pH 7.0–7.5) under λ_{exc} = 390 nm.

We have compared some fluorescent probes that have been reported in recent years for Cu^{2+} ion determination in aqueous samples [24,38–66]. This comparison includes with respect to their working range, operation mode, Stokes shift, as well as interferent metal ions, and can be found in the supplementary information as Table S6. From these data, we can see that in the last five years the number of reported probes working on a Turn-OFF operation mode, as H_2SB showed, is comparable to that working on a Turn-ON mode. Regarding to $\lambda_{ex}/\lambda_{em}$, H_2SB shows large Stokes shift of 110 nm, placing it in that group of probes with minimal interference from self-absorption for Cu^{2+} ions determination [38–41,46,49,50,52,53,55,59,61,63,64]. H_2SB also offers a LOD lower than the majority of the recently reported fluorescence probes for Cu^{2+} ions determination. In addition, its linear working range (0.276–33 μM) is the second widest of those shown in Table S6, and its selectivity is comparable to other recently reported fluorescence probes for Cu^{2+} ions determination.

4. Conclusions

We have synthetized and X-ray characterized a tridentate Schiff base (H_2SB) incorporating a *O,N,N*-binding domain suitable to obtain dinuclear complexes with heavy metal ions such as Cu^{2+}, Zn^{2+}, Ni^{2+}, and Co^{2+} (borderline acids) as well as Pd^{2+} and Cd^{2+} (soft acids). Spectroscopic studies have shown that its complexation towards Cu^{2+}, Zn^{2+}, Ni^{2+}, Co^{2+}, Pd^{2+}, and Cd^{2+} occurred with a 1:1 stoichiometry. Dimeric $Pd_2(SB)_2{\cdot}Me_2CO$, containing a double μ_2–*N*–sulphonamido bridge, showed two pseudo-square planar centers with Pd-N-Pd angles of 93.08(11)° and a Pd–Pd distance of 3.0102(4) Å. This Pd–Pd distance is sensibly shorter than twice the van der Waals radius (4.30 Å), what is a clear indication of a strong palladophilic interaction.

H_2SB emitted fluorescence with a maximum at about 500 nm when it was exposed to UV light with a wavelength of 390 nm. Fluorescence intensity of H_2SB remarkably increases at pH values higher than 11, as a consequence of the deprotonation of its –OH and –SO_2–NH– groups. In aqueous solution, the fluorescence intensity of H_2SB show an increase with increasing concentration of Zn^{2+} and Cd^{2+}. By contrast, addition of Co^{2+}, Ni^{2+}, Pd^{2+} or Cu^{2+}, gave rise to the opposite effect. Quenching of fluorescence by Cu^{2+} occurred as a result of the formation of non-fluorescent ground-state complexes. Binding constant values showed that the affinity of H_2B to borderline acid metal ions, such as Cu^{2+}, Zn^{2+}, Ni^{2+}, and Co^{2+}, is higher than to soft acids, such as Pd^{2+} and Cd^{2+}, but it shows the highest affinity for Cu^{2+}. H_2SB possesses high selectivity toward Cu^{2+}, even in the presence of other common metal ions in water as Na^+, K^+, Ag^+, Mg^{2+}, Ca^{2+}, Ba^{2+}, Mn^{2+}, Fe^{2+}, Co^{2+}, Ni^{2+}, Pd^{2+}, Zn^{2+}, Cd^{2+}, Mn^{3+}, Fe^{3+}, and Al^{3+}, which can be present with a 100 μmol L^{-1} concentration.

Supplementary Materials: Supplementary crystallographic data for this paper have been deposited at Cambridge Crystallographic Data Center (CCDC 1563223 and 1898749) and can be obtained free of charge via www.ccdc.cam.ac.uk/conts/retrieving.html. The following are available online at http://www.mdpi.com/2073-4352/9/8/407/s1, Figures S1–S15: Spectroscopic characterization of the non-crystalline complexes. S16–S17 Additional aspects of the crystal structures determined for this work. Table S1–S5: Diffraction data for H_2SB and $Pd_2(SB)_2Me_2CO$. Figures S18–S23: UV-Vis studies on the H_2SB-M^{n+} interaction. Figures S24–S35: Fluorescence studies on the H_2SB-M^{n+} interaction. Table S6: Comparison of figures of merits of some recently reported fluorescent probes for Cu^{2+} determination.

Author Contributions: Conceptualization, J.S.-M.; methodology, M.Z.-J.; software, A.M.G.-D., J.S.-M., and M.Z.-J.; validation, J.S.-M. and A.M.G.-D.; formal analysis, M.F.; investigation, M.Z.-J.; resources, J.S.-M.; data curation, M.F.; writing—original draft preparation, J.S.-M; writing—review and editing, J.S.-M and A.M.G.-D.; visualisation, M.F.; supervision, J.S.-M.; project administration, J.S.-M.; funding acquisition, J.S.-M.

Funding: This research was funded by the Ministerio de Economía y Competitividad of Spain (Ref. CTQ2015-68094-C2-2-R).

Conflicts of Interest: The authors declare no conflict of interest.

References

1. Campbell, M.G.; Powers, D.C.; Raynaud, J.; Graham, M.J.; Xie, P.; Lee, E.; Ritter, T. Synthesis and structure of solution-stable one-dimensional palladium wires. *Nat. Chem.* **2011**, 949–953. [CrossRef] [PubMed]
2. Mitsumi, M.; Goto, H.; Umebayashi, S.; Ozawa, Y.; Kobayashi, M.; Yokoyama, T.; Tanaka, H.; Kuroda, S.-I.; Toriumi, K. A Neutral Mixed-Valent Conducting Polymer Formed by Electron Transfer between Metal d and Ligand π Orbitals. *Angew. Chem. Int. Ed.* **2005**, *44*, 4164–4168. [CrossRef] [PubMed]
3. Finniss, G.M.; Canadell, E.; Campana, C.; Dunbar, K.R. Unprecedented Conversion of a Compound with Metal–Metal Bonding into a Solvated Molecular Wire. *Angew. Chem. Int. Ed. Engl.* **1996**, *35*, 2772–2774. [CrossRef]
4. Givaja, G.; Castillo, O.; Mateo, E.; Gallego, A.; Gómez-García, C.J.; Calzolari, A.; di Felice, R.; Zamora, F. Electrical Behaviour of Heterobimetallic [MM'(EtCS2)4] (MM' = NiPd, NiPt, PdPt) and MM'X-Chain Polymers [PtM(EtCS$_2$)$_4$I] (M = Ni, Pd). *Chem. Eur. J.* **2012**, *18*, 15476–15484. [CrossRef] [PubMed]
5. Palii, A.V.; Reu, O.S.; Ostrovsky, S.M.; Klokishner, S.I.B.; Tsukerblat, S.; Sun, Z.-M.; Mao, J.-G.; Prosvirin, A.V.; Zhao, H.-H.; Dunbar, K.R. A Highly Anisotropic Cobalt(II)-Based Single-Chain Magnet: Exploration of Spin Canting in an Antiferromagnetic Array. *J. Am. Chem. Soc.* **2008**, *130*, 14729–14738. [CrossRef] [PubMed]
6. Ouellette, W.; Prosvirin, A.V.; Whitenack, K.; Dunbar, K.R.; Zubieta, J.A. Thermally and Hydrolytically Stable Microporous Framework Exhibiting Single-Chain Magnetism: Structure and Properties of [Co$_2$(H$_{0.67}$bdt)$_3$]·20H$_2$O. *Angew. Chem. Int. Ed.* **2009**, *48*, 2140–2143. [CrossRef] [PubMed]
7. Fernández, E.J.; López-de-Luzuriaga, J.M.; Monge, M.; Olmos, M.E.; Pérez, J.; Laguna, A.; Mohamed, A.A.; Fackler, J.P. {Tl[Au(C$_6$Cl$_5$)$_2$]}$_n$: A Vapochromic Complex. *J. Am. Chem. Soc.* **2003**, *125*, 2022–2023. [CrossRef] [PubMed]
8. Mansour, M.A.; Connick, W.B.; Lachicotte, R.J.; Gysling, H.J.; Eisenberg, R. Linear Chain Au(I) Dimer Compounds as Environmental Sensors: A Luminescent Switch for the Detection of Volatile Organic Compounds. *J. Am. Chem. Soc.* **1998**, *120*, 1329–1330. [CrossRef]
9. Lee, Y.-A.; McGarrah, J.E.; Lachicotte, R.J.; Eisenberg, R. Multiple Emissions and Brilliant White Luminescence from Gold(I) *O*,*O*'-Di(alkyl)dithiophosphate Dimers. *J. Am. Chem. Soc.* **2002**, *124*, 10662–10663. [CrossRef]
10. Matthews, R.C.; Howell, D.K.; Peng, W.J.; Laneman, S.A.; Stanley, G.G. Bimetallic Hydroformylation Catalysis: In Situ Characterization of a Dinuclear Rhodium(II) Dihydrido Complex with the Largest Rh–H NMR Coupling Constant. *Angew. Chem. Int. Ed. Engl.* **1996**, *35*, 2253–2256. [CrossRef]
11. Murahashi, T.; Kurosawa, H. Organopalladium complexes containing palladium-palladium bonds. *Coord. Chem. Rev.* **2002**, *231*, 207–228. [CrossRef]
12. Murahashi, T.; Nagai, T.; Mino, Y.; Mochizuki, E.; Kai, Y.; Kurosawa, H. Reversible Interconversion between Dinuclear Sandwich and Half-Sandwich Complexes: Unique Dynamic Behavior of a Pd−Pd Moiety Surrounded by an sp^2-Carbon Framework. *J. Am. Chem. Soc.* **2001**, *123*, 6927–6928. [CrossRef]
13. Werner, H.; Kuhn, A. A General Method for the Synthesis of Sandwich-Type Complexes with a Pd–Pd or Pt–Pt Bond. *Angew. Chem. Int. Ed. Engl.* **1977**, *16*, 412–413. [CrossRef]
14. Sauthier, M.; Le Guennic, B.; Deborde, V.; Toupet, L.; Halet, J.; Réau, R.F. A Rare Phosphane Coordination Mode: A Symmetrically μ_2-Bridging Phosphole in a Dinuclear Palladium(I) Complex. *Angew. Chem. Int. Ed.* **2001**, *40*, 228–231. [CrossRef]
15. Allen, F.H. The Cambridge Structural Database: A quarter of a million crystal structures and rising. *Acta Crystallogr. Sect. B Struct. Sci.* **2002**, *58*, 380–388. [CrossRef]
16. Lasri, J.; Kopylovich, M.N.; da Silva, M.F.C.G.; Charmier, M.A.J.; Pombeiro, A.J.L. Metal-Free and Pd^{II}-Promoted [2+3] Cycloadditions of a Cyclic Nitrone to Phthalonitriles: Syntheses of Oxadiazolines as well as Phthalamide–Pd^{II} and Dihydropyrrolyl-iminoisoindolinone–Pd^{II} Complexes with High Catalytic Activity in Suzuki–Miyaura Cross-Coupling Reactions. *Chem.-Eur. J.* **2008**, *14*, 9312–9322. [CrossRef]
17. Peng, K.-F.; Chen, C.-T. Synthesis, Structural Studies, and Catalytic Application of Palladium Complexes Containing Anilido-Oxazolinate Ligands. *Eur. J. Inorg. Chem.* **2011**, 5182–5195. [CrossRef]
18. Cuevas, J.V.; García-Herbosa, G.; Muñoz, A.; García-Granda, S.; Miguel, D. Metal Complexes of Chiral Imidazolin-2-ylidene Ligands. *Organometallics* **1997**, *16*, 2472–2477. [CrossRef]

19. Beck, B.; Schneider, A.; Freisinger, E.; Holthenrich, D.; Erxleben, A.; Albinati, A.; Zangrando, E.; Randaccio, L.; Lippert, B. Inter- and intra-molecular condensation patterns of (en)Pd^{II} with *trans*-$[a_2PtL_2]^{2+}$ (a = am(m)ine, L = 2-aminopyridine): $PtPd_3$ and Pt_2Pd_4 species with multiple amide bridges. Unexpected trapping of a pair of nitrate ions by a Pt_2Pd_4 double cone. *Dalton Trans.* **2003**, 2533–2539. [CrossRef]
20. Bruns, H.; Patil, M.; Carreras, J.; Vázquez, A.; Thiel, W.; Goddard, R.; Alcarazo, M. Synthesis and coordination properties of nitrogen(I)-based ligands. *Angew. Chem. Int. Ed.* **2010**, *49*, 3680–3683. [CrossRef]
21. Anandhi, U.; Holbert, T.; Lueng, D.; Sharp, P.R. Platinum and Palladium Imido and Oxo Complexes with Small Natural Bite Angle Diphosphine Ligands. *Inorg. Chem.* **2003**, *42*, 1282–1295. [CrossRef]
22. Ruiz, J.; Rodríguez, V.; Cutillas, N.; Florenciano, F.; Pérez, J.; López, G. First complex containing a $Pd_2(\mu_2\text{-}N{=}CPh_2)_2$ functional group. *Inorg. Chem. Commun.* **2001**, *4*, 23–25. [CrossRef]
23. Jess, K.; Baabe, D.; Freytag, M.; Jones, P.G.; Tamm, M. Transition-Metal Complexes with Ferrocene-Bridged Bis(imidazolin-2-imine) and Bis(diaminocyclopropenimine) Ligands. *Eur. J. Inorg. Chem.* **2017**, 412–423. [CrossRef]
24. Sanmartín-Matalobos, J.; García-Deibe, A.M.; Fondo, M.; Zarepour-Jevinani, M.; Domínguez-González, M.R.; Bermejo-Barrera, P. Exploration of an easily synthesized fluorescent probe for detecting copper in aqueous samples. *Dalton Trans.* **2017**, *46*, 15827–15835. [CrossRef]
25. Sanmartín-Matalobos, J.; Portela-García, C.; Fondo, M.; García-Deibe, A.M.; Llamas-Saiz, A.L. A simple route to dinuclear complexes containing unusual $\mu\text{-}\boldsymbol{N}_{\text{sulfonamido}}$ bridges. *J. Coord. Chem.* **2016**, *69*, 1358–1370. [CrossRef]
26. Alvarez, S. A cartography of the van der Waals territories. *Dalton Trans.* **2013**, *42*, 8617–8636. [CrossRef]
27. Sanmartín, J.; Novio, F.; García-Deibe, A.M.; Fondo, M.; Bermejo, M.R. Trimorphism of an asymmetric disulfonamide Schiff base. *New J. Chem.* **2007**, *31*, 1605–1612. [CrossRef]
28. Blessing, R.H. An empirical correction for absorption anisotropy. *Acta Crystallogr. Sect. A Fundam. Crystallogr.* **1995**, *A51*, 33–38. [CrossRef]
29. Sheldrick, G.M. *SADABS, Area-Detector Absorption Correction*; Siemens Industrial Automation, Inc.: Madison, WI, USA, 2001.
30. Sheldrick, G.M. Crystal structure refinement with SHELXL. *Acta Cryst.* **2015**, *C71*, 3–8. [CrossRef]
31. Steiner, T. The Hydrogen Bond in the Solid State. *Angew. Chem. Int. Ed.* **2002**, *41*, 48–76. [CrossRef]
32. García-Deibe, A.M.; Sanmartín-Matalobos, J.; González-Bello, C.; Lence, E.; Portela-García, C.; Martínez-Rodríguez, L.; Fondo, M. Metal-Assisted Ring-Closing/Opening Process of a Chiral Tetrahydroquinazoline. *Inorg. Chem.* **2012**, *51*, 1278–1293. [CrossRef]
33. García-Deibe, A.M.; Portela-García, C.; Fondo, M.; Sanmartín-Matalobos, J. Controlling ring-chain tautomerism through steric hindrance. *RSC Adv.* **2015**, *5*, 58327–58333. [CrossRef]
34. Menabue, L.; Saladini, M. *N*-(arylsulfonyl)glycines as cyclometalating ligands. Crystal and molecular structures of disodium bis(μ-chloro)bis[μ-*N*-(phenylsulfonyl)glycinato-*O*,*N*,*C*]bis[μ-*N*-(phenylsulfonyl)glycinato-*O*,*O*′]tetrapallad hexahydrate and disodium bis(μ-chloro)bis(μ-*N*-tosylglycinato-*O*,*N*,*C*)bis(μ-*N*-tosylglycinato-*O*,*O*′)tetrapalladate(II)-4.5-water-2- *Inorg. Chem.* **1991**, *30*, 1651–1655. [CrossRef]
35. Banerjee, S.; Dixit, A.; Maheswaramma, K.S.; Maity, B.; Mukherjee, S.; Kumar, A.; Karande, A.A.; Chakravarty, A.R. Photocytotoxic ternary copper (II) complexes of histamine Schiff base and pyridyl ligands. *J. Chem. Sci.* **2016**, *128*, 165–175. [CrossRef]
36. Lakowicz, J.R. *Principles of Fluorescence Spectroscopy*, 3rd ed.; Springer: New York, NY, USA, 2006.
37. Kim, H.M.; Jung, C.; Kim, B.R.; Jung, S.-Y.; Hong, J.H.; Ko, Y.-G.; Lee, K.J.; Cho, B.R. Environment-sensitive two-photon probe for intracellular free magnesium ions in live tissue. *Angew. Chem. Int. Ed.* **2007**, *46*, 3460–3463. [CrossRef]
38. Uyanik, I.; Oguz, M.; Bhatti, A.A.; Uyanik, A.; Yilmaz, M. A New Piperidine Derivatized-Schiff Base Based "Turn-on" Cu^{2+} Chemo-Sensor. *J. Fluoresc.* **2017**, *27*, 791–797. [CrossRef]
39. Situ, B.; Zhao, J.; Lv, W.; Li, J.; Li, H.; Li, B.; Chai, Z.; Cao, N.; Zheng, L. Naked-eye detection of copper(II) ions by a "clickable" fluorescent sensor. *Sens. Actuators B Chem.* **2017**, *240*, 560–565. [CrossRef]
40. Saleh, S.M.; Ali, R.; Ali, I.A.I. A novel, highly sensitive, selective, reversible and turn-on chemi-sensor based on Schiff base for rapid detection of Cu(II). *Spectrochim. Acta A Mol. Biomol. Spectrosc.* **2017**, *183*, 225–231. [CrossRef]

41. Parthiban, C.; Elango, K.P. Design, synthesis, characterization and cation sensing behavior of amino-naphthoquinone receptor: Selective colorimetric sensing of Cu(II) ion in nearly aqueous solution with mimicking logic gate operation. *Spectrochim. Acta Part A Mol. Biomol. Spectrosc.* **2017**, *174*, 147–153. [CrossRef]
42. Vanlı, E.; Mısır, M.N.; Alp, H.; Ak, T.; Özbek, N.; Ocak, Ü.; Ocak, M. Ion Sensor Properties of Fluorescent Schiff Bases Carrying Dipicolylamine Groups. A Simple Spectrofluorimetric Method to Determine Cu (II) in Water Samples. *J. Fluoresc.* **2017**, *27*, 1759–1766. [CrossRef]
43. Roy, N.; Dutta, A.; Mondal, P.; Paul, P.C.; Singh, T.S. Coumarin Based Fluorescent Probe for Colorimetric Detection of Fe3+ and Fluorescence Turn On-Off Response of Zn^{2+} and Cu^{2+}. *J. Fluoresc.* **2017**, *27*, 1307–1321. [CrossRef]
44. Wu, Q.; Ma, L.; Xu, Y.; Cao, D.; Guan, R.; Liu, Z.; Yu, X. Two coumarin formhydrazide compounds as chemosensors for copper ions. *Inorg. Chem. Commun.* **2016**, *69*, 7–9. [CrossRef]
45. Khaokeaw, C.; Sukwattanasinitt, M.; Rashatasakhon, P. Salicylyl Fluorene Derivatives as Fluorescent Sensors for Cu(II) Ions. *J. Fluoresc.* **2016**, *26*, 745–752. [CrossRef]
46. Thavornpradit, S.; Sirirak, J.; Wanichacheva, N. Turn-on naphthalimide fluorescent sensor with high quantum yield and large Stokes shift for the determination of Cu (II). *J. Photochem. Photobiol. A Chem.* **2016**, *330*, 55–63. [CrossRef]
47. Tümay, S.O.; Okutan, E.; Sengul, I.F.; Özcan, E.; Kandemir, H.; Doruk, T.; Çetin, M.; Çosut, B. Naked-eye fluorescent sensor for Cu (II) based on indole conjugate BODIPY dye. *Polyhedron* **2016**, *117*, 161–171. [CrossRef]
48. Gao, Y.; Li, Y.; Yang, X.; He, F.; Huang, J.; Jiang, M.; Zhou, Z.; Chen, H. Design, synthesis and biological evaluation of a novel Cu 2+-selective fluorescence sensor for bio-detection and chelation. *RSC Adv.* **2015**, *5*, 80110–80117. [CrossRef]
49. Zhang, Y.; Guo, X.; Tian, X.; Liu, A.; Jia, L. Carboxamidoquinoline–coumarin derivative: A ratiometric fluorescent sensor for Cu (II) in a dual fluorophore hybrid. *Sens. Actuators B Chem.* **2015**, *218*, 37–41. [CrossRef]
50. Aggarwal, K.; Khurana, J.M. Phenazine containing indeno-furan based colorimetric and "on–off" fluorescent sensor for the detection of Cu^{2+} and Pb^{2+}. *J. Lumin.* **2015**, *167*, 146–155. [CrossRef]
51. Maher, N.J.; Diao, H.; O'sullivan, J.; Fadda, E.; Heaney, F.; McGinley, J. Lower rim isoxazole-calix [4] arene derivatives as fluorescence sensors for copper (II) ions. *Tetrahedron* **2015**, *71*, 9223–9233. [CrossRef]
52. Ganguly, A.; Ghosh, S.; Kar, S.; Guchhait, N. Selective fluorescence sensing of Cu(II) and Zn(II) using a simple Schiff base ligand: Naked eye detection and elucidation of photoinduced electron transfer (PET) mechanism. *Spectrochim. Acta A* **2015**, *143*, 72–80. [CrossRef]
53. Kumar, J.; Bhattacharyya, P.K.; Das, D.K. New duel fluorescent "on–off" and colorimetric sensor for copper (II): Copper (II) binds through N coordination and pi cation interaction to sensor. *Spectrochim. Acta A* **2015**, *138*, 99–104. [CrossRef]
54. Wagh, Y.B.; Kuwar, A.; Sahoo, S.K.; Galluccic, J.; Dalal, D.S. Highly selective fluorimetric sensor for Cu 2+ and Hg 2+ using a benzothiazole-based receptor in semi-aqueous media and molecular docking studies. *RSC Adv.* **2015**, *5*, 45528–45534. [CrossRef]
55. Erdemir, S.; Malkondu, S. Novel "turn on" fluorescent sensors based on anthracene and carbazone units for Cu (II) ion in CH_3CN–H_2O. *J. Lumin.* **2015**, *158*, 86–90. [CrossRef]
56. Gunduz, Z.Y.; Gunduz, C.; Ozpınar, C.; Urucu, O.A. A novel Schiff-base as a Cu (II) ion fluorescent sensor in aqueous solution. *Spectrochim. Acta A* **2015**, *136*, 1679–1683. [CrossRef]
57. Huang, C.-B.; Li, H.-R.; Luo, Y.; Xu, L. A naphthalimide-based bifunctional fluorescent probe for the differential detection of Hg^{2+} and Cu^{2+} in aqueous solution. *Dalton Trans.* **2014**, *43*, 8102–8108. [CrossRef]
58. Fu, Y.; Tian, Q.-F.; Guo, Y.-Q.; Zang, S.-Q. New rhodamine-based turn-on and colorimetric probe for copper(II) ion with high selectivity and sensitivity. *Inorg. Chim. Acta* **2014**, *419*, 141–146. [CrossRef]
59. Mukherjee, S.; Mal, P.; Stoeckli-Evans, H. Hydrazone based luminescent receptors for fluorescent sensing of Cu^{2+}: Structure and spectroscopy. *J. Lumin.* **2014**, *155*, 185–190. [CrossRef]
60. Kao, S.-L.; Lin, W.-Y.; Venkatesan, P.; Wu, S.-P. Colorimetric detection of Cu(II): Cu(II)-induced deprotonation of NH responsible for color change. *Sens. Actuators B Chem.* **2014**, *204*, 688–693. [CrossRef]

61. Kumbhar, H.S.; Yadav, U.N.; Gadilohar, B.L.; Shankarling, G.S. A highly selective fluorescent chemosensor based on thio-β-enaminone analog with a turn-on response for Cu(II) in aqueous media. *Sens. Actuators B Chem.* **2014**, *203*, 174–180. [CrossRef]
62. Puangploy, P.; Smanmoo, S.; Surareungchai, W. A new rhodamine derivative-based chemosensor for highly selective and sensitive determination of Cu^{2+}. *Sens. Actuators B Chem.* **2014**, *193*, 679–686. [CrossRef]
63. Qazi, M.A.; Ocak, Ü.; Ocak, M.; Memon, S. An excellent copper selective chemosensor based on calix [4] arene framework. *Anal. Chim. Acta* **2013**, *761*, 157–168. [CrossRef]
64. Tang, L.; Zhou, P.; Zhang, Q.; Huang, Z.; Zhao, J.; Cai, M. A simple quinoline derivatized thiosemicarbazone as a colorimetic and fluorescent sensor for relay recognition of Cu^{2+} and sulfide in aqueous solution. *Inorg. Chem. Commun.* **2013**, *36*, 100–104. [CrossRef]
65. Tang, L.; Cai, M.; Huang, Z.; Zhong, K.; Hou, S.; Bian, Y.; Nandhakumar, R. Rapid and highly selective relay recognition of Cu(II) and sulfide ions by a simple benzimidazole-based fluorescent sensor in water. *Sens. Actuators B Chem.* **2013**, *185*, 188–194. [CrossRef]
66. Tang, L.; Zhou, P.; Zhong, K.; Hou, S. Fluorescence relay enhancement sequential recognition of Cu^{2+} and CN^{-} by a new quinazoline derivative. *Sens. Actuators B Chem.* **2013**, *182*, 439–445. [CrossRef]